Proceedings of 2013 IEEE
International Conference on Mechatronics and Automation
August 4 - 7, Takamatsu, Japan

Robust Trajectory Linearization Control of a Flexible Hypersonic Vehicle in the Presence of Uncertainties

Zhiqiang Pu, Xiangmin Tan, Guoliang Fan, and Jianqiang Yi
Institute of Automation, Chinese Academy of Sciences, Beijing, 100190,China
zhiqiang.pu@ia.ac.cn

***Abstract* – This paper addresses the design of a robust trajectory linearization control (TLC) scheme for a flexible air-breathing hypersonic vehicle model with multiple uncertainties. Because of the model complexity, the flexibility effects and open-loop behaviors are analyzed, offering insights on the vehicle features and guidelines for control design. Based on the analysis, a basic TLC frame, including an adaptive time-varying bandwidth algorithm, is firstly constructed. As for the inevitable uncertainties in hypersonic flight, a uniform nonlinear uncertainty model is explored which lumps all external disturbances and typical internal uncertainties such as propulsive perturbations and variations in control effectiveness together. Then extended state observer (ESO) technique is integrated into the basic TLC frame to estimate and compensate these uncertainties, forming a robust TLC scheme. Two flight cases are conducted, through which the robust scheme exhibits great tracking performance and uncertainty rejection ability.**

Index Terms* – *Trajectory Linearization Control, Flexible, Hypersonic Vehicle, Uncertainty, Extended State Observer

I. Introduction

Air-breathing hypersonic vehicles are viewed as a reliable and cost-effective solution to access to space routine. Since the 1960s, considerable efforts have been made to develop practical and affordable vehicles, such as NASA X-43A and U. S. Air Force X-51A. However, the design of robust guidance and control systems is still a challenging task due to the complex features of the vehicle dynamics [1]-[8]. Hypersonic flight usually covers a large flight envelope during which the environmental and aerodynamic characteristics undergo huge variations. The slender geometries and light structures required for these aircraft cause significant flexible effects. Strong interactions also exist among propulsion, structure, aerodynamics, and control. In addition, diverse uncertainties must be accommodated.

In recent literature, there are two dominant flexible air-breathing hypersonic vehicle (FAHV) models: one is the first-principle model developed by Bolender and Doman [1], the other is the computational fluid dynamics (CFD) based model of Mirmirani et al. [2]. For the first model, linear approaches were applied for control design in [3]-[4], while nonlinear methods were investigated in [5]-[6]. For the second model, [7] developed an adaptive linear quadratic controller, while [8] presented a control scheme that could suppress unknown or changing flexible modes online. Despite these research results, the design of robust control systems is still an open problem because of the peculiarity of the vehicle dynamics [6]. In this paper, we utilize the trajectory linearization control (TLC) [9]-[12] method to solve this problem. As a novel nonlinear control approach, TLC can inherently guarantee exponential stability of the closed-loop system along nominal trajectories using linear time-varying (LTV) system spectral theory [12]. Moreover, TLC provides a unique time-varying bandwidth (TVB) technique to feasibly improve the control performance and system robustness, which distinguishes it from other nonlinear control methods.

Uncertainties are inevitable during practical FAHV flight. This issue is considered in many papers [3]-[5] with varying levels of uncertainties. In these papers, however, uncertainties were only applied to test the inherent system robustness and no particular technique was adopted to deal with them. For a model based control method, in order to design a controller that owns the best uncertainty rejection ability, a valid uncertainty model is assumed to be available. Buschek et al. [13] presented a uniform model which could represent a large class of uncertainties, but it was in a simple linear form. In this paper, we develop a uniform nonlinear uncertainty model that is more realistic for FAHV. Multiple uncertainty sources are considered, including external disturbances such as wind gusts and two typical internal hypersonic effects, i.e. propulsive perturbations and variations in control effectiveness. Instead of overcoming the uncertainties by the inherent system robustness, we incorporate extended state observer (ESO) [14]-[15] into a basic TLC frame to estimate and compensate the uncertainties. Compared with other estimation techniques such as fuzzy logic and neural network, ESO shows multiple advantages such as high efficiency and satisfying flexibility. Its great simplicity can also meet the fast computation requirements in hypersonic missions.

To sum up, in this paper we design a robust TLC scheme for FAHV under multiple uncertainties. It incorporates a basic TLC frame (including an adaptive TVB algorithm) with ESO technique. In addition, a uniform uncertainty model is proposed for convenience of controller synthesis.

II. Vehicle Model Description and Analysis

A. Vehicle Model

The vehicle studied in this paper is the model developed by Bolender and Doman [1] for the longitudinal dynamics of a FAHV. Flexibility effects are included by modeling the fuselage as two cantilever beams clamped at the center of gravity, rather than a single free-free beam as done in [3]. This vibrational model captures the inertial coupling between the

978-1-4673-5560-5/13/$31.00 ©2013 IEEE

rigid-body states and the flexible states, resulting in a system that is more complex to control [1]. Assuming a flat Earth and normalizing the vehicle to unit depth, the longitudinal sketch of the vehicle is illustrated in Fig. 1, and the equations of motion are written as [5]

$$\dot{V} = (T\cos\alpha - D)/m - g\sin\gamma \tag{1}$$

$$\dot{\gamma} = (L + T\sin\alpha)/(mV) - g\cos\gamma/V \tag{2}$$

$$\dot{h} = V\sin\gamma \tag{3}$$

$$\dot{\alpha} = Q - \dot{\gamma} \tag{4}$$

$$I_{yy}\dot{Q} = M + \tilde{\psi}_f\ddot{\eta}_f + \tilde{\psi}_a\ddot{\eta}_a \tag{5}$$

$$k_f\ddot{\eta}_f = -2\xi_f\omega_f\dot{\eta}_f - \omega_f^2\eta_f + N_f - \tilde{\psi}_f M/I_{yy} - \tilde{\psi}_f\tilde{\psi}_a\ddot{\eta}_a/I_{yy} \tag{6}$$

$$k_a\ddot{\eta}_a = -2\xi_a\omega_a\dot{\eta}_a - \omega_a^2\eta_a + N_a - \tilde{\psi}_a M/I_{yy} - \tilde{\psi}_a\tilde{\psi}_f\ddot{\eta}_f/I_{yy} \tag{7}$$

This model is composed of five rigid-body state variables $x=[V,\gamma,h,\alpha,Q]^T$, where V,γ,h,α,Q are the velocity, flight-path angle, altitude, angle of attack, and pitch rate, respectively. It also includes four flexible states $\eta=[\eta_f,\dot{\eta}_f,\eta_a,\dot{\eta}_a]^T$ which correspond to the first generalized elastic deformations and their derivatives of the forebody (denoted with subscript f) and aftbody (denoted with subscript a). The outputs to be controlled are selected as $y=[V,h]^T$. The elevator deflection δ_e and the fuel equivalence ratio ϕ construct the control inputs $u=[\delta_e,\phi]^T$, which indirectly affects the vehicle states through the lift L, drag D, thrust T, pitching moment M, and the generalized forces N_f and N_a. Readers may refer to [5] for a full description of the model variables.

The aforementioned forces and moments are complex nonlinear functions of the vehicle states and control inputs. Therefore, [5] developed a curve-fitted model (CFM) to approximate these forces and moments, which is described as

$$\begin{cases} L \approx \bar{q}SC_L(\alpha,\delta_e), \quad D \approx \bar{q}SC_D(\alpha,\delta_e) \\ T \approx C_T^{\alpha^3}\alpha^3 + C_T^{\alpha^2}\alpha^2 + C_T^{\alpha}\alpha + C_T^0 \\ M \approx z_T T + \bar{q}S\bar{c}[C_{M,\alpha}(\alpha) + C_{M,\delta_e}(\delta_e)] \\ N_f \approx N_f^{\alpha^2}\alpha^2 + N_f^{\alpha}\alpha + N_f^0,\ N_a \approx N_a^{\alpha^2}\alpha^2 + N_a^{\alpha}\alpha + N_a^{\delta_e}\delta_e + N_a^0 \end{cases} \tag{8}$$

The coefficients are expressed as

$$\begin{cases} C_L = C_L^{\alpha}\alpha + C_L^{\delta_e}\delta_e + C_L^0 \\ C_D = C_D^{\alpha^2}\alpha^2 + C_D^{\alpha}\alpha + C_D^{\delta_e^2}\delta_e^2 + C_D^{\delta_e}\delta_e + C_D^0 \\ C_{M,\alpha} = C_{M,\alpha}^{\alpha^2}\alpha^2 + C_{M,\alpha}^{\alpha}\alpha + C_{M,\alpha}^0, \quad C_{M,\delta_e} = c_e\delta_e \\ C_T^{\alpha^3} = \beta_1(h,\bar{q})\phi + \beta_2(h,\bar{q}), \quad C_T^{\alpha^2} = \beta_3(h,\bar{q})\phi + \beta_4(h,\bar{q}) \\ C_T^{\alpha} = \beta_5(h,\bar{q})\phi + \beta_6(h,\bar{q}), \quad C_T^0 = \beta_7(h,\bar{q})\phi + \beta_8(h,\bar{q}) \end{cases} \tag{9}$$

where $\bar{q}=0.5\rho V^2$ denotes the dynamic pressure. The air density ρ is modeled as $\rho=\rho_0\exp(-h/h_0)$, and the actuators are modeled as first-order low-pass filters with certain gains. Limits on the control inputs are set as

$$-15\,\text{deg} \le \delta_e \le 15\,\text{deg}, \quad 0.1 \le \phi \le 1.2 \tag{10}$$

B. *Flexibility Effects Analysis*

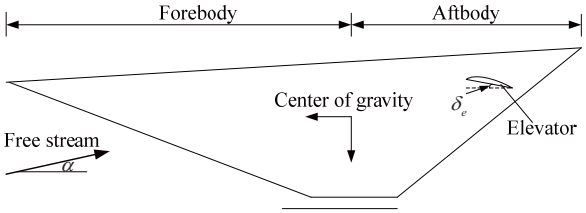

Fig. 1 Geometry of the hypersonic vehicle model.

The slender geometries and light structures of FAHV cause significant flexibility effects that severely affect the aerodynamics of the aircraft. Three factors that determine the ith flexible mode effects are the frequency ω_i, damping ratio ξ_i, and mode shape ϕ_i. Here, for all modes the damping ratio is constant $\xi_i = 0.02$ as done in [3]-[4], which indicates a severe mode vibration condition. The other two factors, however, need to be carefully analyzed. Particularly, the fuel is consumed during hypersonic flight, which has a significant impact on the structural dynamics. In the following analysis, we will find out how the mode shape and frequency change with four different fuel levels. The corresponding vehicle mass densities are listed in Table I.

In the nominal case (Case 1), mode shapes for the first three flexible modes are shown in Fig. 2a. It is seen that, as the fuselage is modeled as two cantilever beams clamped at the center of gravity (55 ft away from the nose), the displacement and rotation there are zero. This is different from the free-free model in [3]. Fig. 2b shows the second mode shape with mass density ranging from 300 slugs/ft to 150 slugs/ft. As a general rule, the displacement increases as the mass density decreases, resulting in changes of the vehicle dynamics. Besides the second mode shape, all other mode shapes lead to the same rule. This means lighter vehicle structures or more fuel consumption cause larger flexibility effects. As for the mode frequency, similar analysis indicates that increased mass density leads to decreased flexible mode frequencies. If the decreasing flexible frequencies approach to the natural frequency of the rigid body, significant coupling occurs and the vehicle dynamics become more complex.

TABLE I MASS DENSITIES UNDER VARYING FUEL LEVELS

Fuel level	Case 1	Case 2	Case 3	Case 4
Mass (slugs/ft)	300	250	200	150

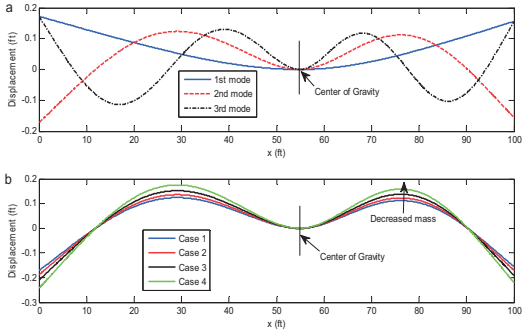

Fig. 2 Mode shapes: a. the first three mode shapes in nominal case; b. the second mode shape with varying mass densities.

C. Open-loop Analysis

FAHV exhibits complex time-varying coupling effects not only between the rigid and flexible states, but also between the aerodynamics and environment. A key factor that affects the vehicle feature is the dynamic pressure $\bar{q}$, which influences all the forces and moments. For this reason, an open-loop analysis is conducted with $\bar{q}$ ranging from 2000 psf to 500 psf. We trim the vehicle at each $\bar{q}$ level, and then linearize it at the trim conditions. Fig. 3 shows how the poles and zeros of the linearized system migrate as $\bar{q}$ changes. As expected, three poles corresponding to the phugoid and altitude modes are near the origin. The two complex conjugate pairs correspond to the flexible dynamics. The pair of poles and zeros that appear to be symmetric about the imaginary axis correspond to the rotational dynamics (the angle of attack and pitch rate). There is an unstable pole, which complicates the control design. As the dynamic pressure decreases, both the positive and negative poles migrate to the origin. This is reasonable because with a smaller $\bar{q}$ all forces and moments decrease. On one hand, it makes the unstable dynamics much milder; on the other hand, it yields a larger oscillation in the stable dynamics. Finally, the positive zero indicates a nonminimum phase behavior, which stems from the coupling of the elevator to the lift and drag forces. This phenomenon was also reported in [5] and [6], where an additional canard was therefore added to deal with it.

III. Robust Scheme Design

In this section, the robust scheme is designed for FAHV. The starting point is to decompose the equations of motion into functional subsystems. Based on the time-scale separation theory, the vehicle dynamics are divided into five subsystems, i.e. the velocity, altitude, flight-path angle (FPA), angle of attack (AOA), and pitch rate subsystems. Five subsystem controllers are designed correspondingly. The overall scheme is depicted in Fig. 4, where the virtual control inputs are drawn as dashed lines. Feedback lines are omitted for simplicity. Fig. 5 shows the structure of each robust controller, which mainly consists of a basic TLC frame and an ESO. The TLC frame contains a pseudo-inversion and a stabilizing controller, constructing a basic control law; the ESO estimates the uncertainties to form a compensation control law.

A. Basic TLC Frame Design

Mostly, the control objective is to design a control law that drives the system output to track a nominal output trajectory. In TLC frame, the original system is firstly linearized along the nominal trajectory, thus the tracking problem is cast into a regulation problem for the error dynamics along the nominal trajectory. Asymptotic tracking can then be achieved by combining a feed-forward pseudo inversion of the nominal model and a feedback stabilizer of the linearized tracking error dynamics, as shown in the dashed box of Fig. 5.

A.1 TLC for the Velocity Subsystem

In view of the force expressions in (8)-(9), the velocity dynamics (1) can be rewritten as an affine form:

$$\dot{V} = f_V + g_V u_V \tag{11}$$

where

$$f_V = [(\beta_2\alpha^3 + \beta_4\alpha^2 + \beta_6\alpha + \beta_8)\cos\alpha - D]/m - g\sin\gamma$$

$$g_V = (\beta_1\alpha^3 + \beta_3\alpha^2 + \beta_5\alpha + \beta_7)\cos\alpha / m, \quad u_V = \phi$$

Denote the nominal velocity to be tracked as $\bar{V}$, and replace V by $\bar{V}$ in f_V and g_V , yielding $\bar{f}_V$ and $\bar{g}_V$ correspondingly. Assume $\bar{g}_V$ is invertible. Then a nominal control law $\bar{u}_V$ can be obtained by the pseudo inversion:

$$\bar{u}_V = \bar{g}_V^{-1}(\dot{\bar{V}} - \bar{f}_V) \tag{12}$$

Here $\dot{\bar{V}}$ is generated by a command processor as shown in Fig. 5. Another effect of this command processor is to make the given command more realizable. In this paper, the command processor is designed by the arranged transient process (ATP) technique [14]-[15]. The detail of ATP is omitted here to avoid clouding the primary ideas of this paper.

To design the stabilizing controller, system (11) is first augmented with integral action for disturbance accommodation and performance enhancement. Defining the augmented state $x_V = [\int V dt, V]^T$ yields the augmented system as

$$\dot{x}_V = [V, f_V]^T + [0, g_V]^T u_V \tag{13}$$

Stabilizing feedback control is implemented by first defining the velocity tracking error as $e_V = x_V - \bar{x}_V$ where $\bar{x}_V = [\int \bar{V} dt, \bar{V}]^T$ is the nominal state, and then linearizing the tracking-error system along the nominal state. The linearized LTV tracking error system is written as

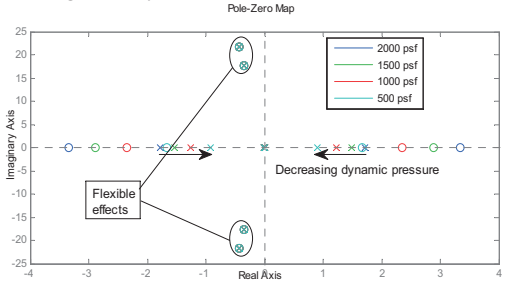

Fig. 3 Pole-zero map with varying dynamic pressure.

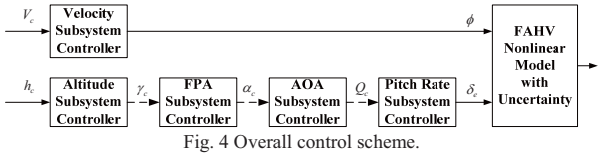

Fig. 4 Overall control scheme.

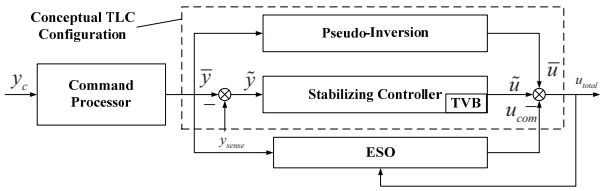

Fig. 5 Structure for each robust controller.

$$\dot{e}_V = A_V(t)e_V + B_V(t)\tilde{u}_V \tag{14}$$

where

$$A_V(t) = \begin{bmatrix} 0 & 1 \\ 0 & -\rho\bar{V}SC_D / m \end{bmatrix},\ B_V(t) = \begin{bmatrix} 0 \\ \bar{g}_V \end{bmatrix},\ \tilde{u}_V = u_V - \bar{u}_V$$

Select the feedback control law as

$$\tilde{u}_V = K_V(t)e_V = \left[k_{V1}(t), k_{V2}(t)\right]e_V \tag{15}$$

where $k_{V1}(t), k_{V2}(t)$ are the control gains. Then assume the desired closed-loop system matrix $A_{Vc}(t)$ as

$$A_{Vc}(t) = \begin{bmatrix} 0 & 1 \\ -\tau_{V1}(t) & -\tau_{V2}(t) \end{bmatrix}$$

LTV PD-spectral theory [12] is adopted to assign the desired dynamics as

$$\begin{cases} \tau_{V1}(t) = \omega_{Vn}^2(t) \\ \tau_{V2}(t) = 2\xi_V\omega_{Vn}(t) - \dot{\omega}_{Vn}(t) / \omega_{Vn}(t) \end{cases} \tag{16}$$

Then according to $A_V + B_V K_V = A_{Vc}$, the control gains are computed as

$$k_{V1}(t) = -\tau_{V1}(t),\ k_{V2}(t) = -\tau_{V2}(t) + \rho\bar{V}SC_D / m$$

and the feedback control law (15) is obtained.

The total TLC control law of the velocity subsystem is

$$u_V = \bar{u}_V + \tilde{u}_V \tag{17}$$

In (16), the constant damping ratio ξ_V and time-varying bandwidth $\omega_{Vn}(t)$ are the direct parameters to be tuned. To improve the control performance, we design an adaptive TVB algorithm for $\omega_{Vn}(t)$, which is addressed later.

A.2 TLC for Other Subsystems

Control design for the velocity subsystem exhibits a standard TLC design procedure, which can be concluded into six steps: a) write the original dynamics into an affine form; b) calculate the pseudo inversion control law; c) augment the original dynamics with integral actions; d) linearize the tracking-error system along nominal trajectories; e) assign the desired closed-loop dynamics with PD-spectral theory and obtain the stabilizing control law; f) add the pseudo inversion control and the stabilizing control to form the total control law. These six steps can be similarly applied to other four subsystems. Due to page limitation, detailed design procedure is omitted here. Note that some subsystems cannot be directly written into affine forms, thus approximation must be made. The flexible effects are included in the pitch rate subsystem, thus are well suppressed by the robust scheme.

A.3 Adaptive TVB Algorithm

As stated in the open-loop analysis, the dynamic pressure $\bar{q}$ has a great impact on the vehicle characteristics. In large velocity or altitude maneuvers, $\bar{q}$ may experience huge variations. To enhance the system robustness and tracking performance, we design an adaptive TVB algorithm as

$$\omega_n(t) = \omega_{n0}\sqrt{\bar{q} / \bar{q}_0} \tag{18}$$

where ω_{n0} and $\bar{q}_0$ are the bandwidth and dynamic pressure at an initial trim condition. The physical interpretation of (18) lies in that, with an increasing dynamic pressure all forces and moments increase, which makes all flight dynamics change faster, thus the relative bandwidth should be increased; and vice versa. With the stability analysis in [10], it can be proved that TVB algorithm (18) can overcome a larger disturbance and yield a smaller tracking error.

As shown in Fig. 3, $\bar{q}$ significantly affects the rotational dynamics. Thus this adaptive TVB algorithm is primarily applied to the angle of attack and pitch rate subsystems.

B. Uncertainty Modeling

Recall the force/moment expressions (8)-(9). Three variables that primarily determine the forces and moments are the flight state α and the control inputs δ_e and ϕ, so sensitivities to variations of these variables become three primary internal uncertainty sources. Meanwhile, external disturbance such as wind gusts should also be considered. For the rigid body, all these uncertainties can be represented by this nonlinear uncertain model

$$\dot{x} = f(x,u) + f_{\Delta i}(x,u,t) + f_{\Delta e}(x,u,t) \tag{19}$$

where $\dot{x} = f(x,u)$, $x \in \Re^5$, represents the nominal dynamics (1)-(5), while $f_{\Delta i}(x,u,t), f_{\Delta e}(x,u,t)$ denote the total internal and external uncertainties, respectively.

Denote the total number of internal uncertainty cases as n_Δ. Then $f_{\Delta i}(x,u,t)$ can be expressed as

$$f_{\Delta i}(x,u,t) = \sum_{k=1}^{n_\Delta} f_{\Delta i}^k(x,u,t) \tag{20}$$

For each internal uncertainty $f_{\Delta i}^k(x,u,t) \in \Re^5$, it is modeled as

$$\begin{cases} e_{\Delta k} = A_{\Delta k}^T F_1(\Delta_{lk}) B_{\Delta k} \\ f_{\Delta i}^k(x,u,t) = F_2(e_{\Delta k}) A_{\Delta k} \end{cases} \tag{21}$$

Here, Δ_{lk} denotes the uncertainty level. Constant vectors $A_{\Delta k} \in \Re^{4\times 1}$ and $B_{\Delta k} \in \Re^{3\times 1}$ are chosen to "pick out" the matched uncertainty source and the disturbed dynamics. $F_1 \in \Re^{4\times 3}$ describes how the three primary internal uncertainty sources affect the four forces/moments, while $F_2 \in \Re^{5\times 4}$ tells how the four forces/moments affect the five rigid-body states. Both F_1 and F_2 have fixed forms which are separately derived from the force/moment expressions (8)-(9) and the equations of motion (1)-(5). They are expressed as

$$F_1 = \begin{bmatrix} L_\alpha & L_{\delta_e} & 0 \\ D_\alpha & D_{\delta_e} & 0 \\ T_\alpha & 0 & T_\phi \\ M_\alpha & M_{\delta_e} & M_\phi \end{bmatrix},\ F_2 = \begin{bmatrix} 0 & V_D & V_T & 0 \\ \gamma_L & 0 & \gamma_T & 0 \\ 0 & 0 & 0 & 0 \\ \alpha_L & 0 & \alpha_T & 0 \\ 0 & 0 & 0 & Q_M \end{bmatrix} \tag{22}$$

For example, M_α in F_1 describes how the variation of α affects the pitching moment M, while Q_M in F_2 tells how the disturbed M affects the pitch rate Q. According to (8)-(9) and (1)-(5), they are calculated as

$$M_\alpha(\Delta_{lk}) = [\bar{q}S\bar{c}(C_{M,\alpha}^{\alpha^2}\alpha^2 + C_{M,\alpha}^{\alpha}\alpha) + C_T^{\alpha^3}\alpha^3 + C_T^{\alpha^2}\alpha^2 + C_T^{\alpha}\alpha]\Delta_{lk} \tag{23}$$

$$Q_M(e_{\Delta k}) = e_{\Delta k} / I_{yy} \tag{24}$$

Expressions of other elements are omitted for brevity.

FAHV utilizes scramjet propulsion system which is highly integrated into the airframe. This results in an increased sensitivity to variations in angle of attack. Subsequently, the pitching moment is affected, leading to significant disturbance to the pitch rate dynamics. This effect is taken as internal uncertainty in the pitching moment sensitivity to angle of attack variations. Accordingly, we set the constant vectors as $A_{\Delta 1}=[0,0,0,1]^T$, $B_{\Delta 1}=[1,0,0]^T$ to pick out M_α and Q_M as expressed in (23)-(24) to model this propulsive perturbation.

Besides the propulsion uncertainty, another internal uncertainty lies in the control effectiveness variations, which are modeled as uncertainties in pitching moment sensitivity to elevator deflection and in thrust sensitivity to fuel equivalence ratio. These two uncertainties are included by separately setting $A_{\Delta 2}=[0,0,0,1]^T$, $B_{\Delta 2}=[0,1,0]^T$ and $A_{\Delta 3}=[0,0,1,0]^T$, $B_{\Delta 3}=[0,0,1]^T$.

As for the external uncertainty $f_{\Delta e}(x,u,t)$, it may results from wind gusts or other environmental uncertainties. For demonstration, it is chosen as sine wave signals [4]

$$f_{\Delta e}(x,u,t)=[2\sin t,\,5\cos t,\,0.3\sin t,\,0.3\sin t,\,0.02\sin t\,]^T \quad (25)$$

C. Extended State Observer Design

Perturbation analysis shows that the basic TLC frame can guarantee local exponential stability only when perturbation is limited in a specified range [10]. To enhance the system robustness, nonlinear ESO [14] is integrated with the basic TLC frame for uncertainty compensation. The core idea of ESO is to take all internal and external uncertainties modeled above as a new extended state, and then establish a state observer to estimate these uncertainties.

Assume the disturbed velocity dynamics are written as

$$\dot{V}=f_V+g_V u_V+\Delta_V \quad (26)$$

with Δ_V denotes the total uncertainty. Let $x_{V1}=V, x_{V2}=\Delta_V$, where x_{V2} is an extended state. Suppose $\dot{\Delta}_V$=-$w_V(t)$ with $w_V(t)$ unknown but bounded. Then (26) can be written as a second-order extended system:

$$\dot{x}_{V1}=f_V+g_V u_V+x_{V2},\quad \dot{x}_{V2}=-w_V(t) \quad (27)$$

An ESO is established for (27) as

$$\begin{cases}\dot{z}_{V1}=f_V+g_V u_V+z_{V2}-\beta_{V1}\tilde{z}_V\\ \dot{z}_{V2}=-\beta_{V2}\,fal(\tilde{z}_V,\alpha_V,\delta_V)\end{cases} \quad (28)$$

where $\tilde{z}_V=z_{V1}-x_{V1}$ denotes the estimation error, z_{Vi} is the estimation value of x_{Vi}, and β_{Vi} is the observing gain, $i=1,2$. fal is a nonlinear function of $\tilde{z}_V$, expressed as [14]

$$fal(\tilde{z}_V,\alpha_V,\delta_V)=\begin{cases}|\tilde{z}_V|^{\alpha_V}\cdot sign(\tilde{z}_V), & |\tilde{z}_V|>\delta_V\\ \tilde{z}_V/\delta^{1-\alpha_V}, & |\tilde{z}_V|\le\delta_V\end{cases} \quad (29)$$

where δ_V,α_V are constants with $\delta_V>0$ and $0<\alpha_V<1$. By properly choosing the parameters β_{V1}, β_{V2}, α_V, and δ_V, we have $z_{V1}\to V$, $z_{V2}\to\Delta_V$. Then a compensation control law is obtained as

$$u_{Vcom}=g_V^{-1}z_{V2} \quad (30)$$

This together with the basic TLC control law (17) produces the final robust control law for the velocity subsystem:

$$u_V=\bar{u}_V+\tilde{u}_V-u_{Vcom} \quad (31)$$

IV. Simulations

To illustrate the effectiveness of the proposed robust TLC scheme, two representative flight cases for this FAHV are studied: a climbing maneuver at constant dynamic pressure (Case 1) and a climbing maneuver with longitudinal acceleration using separate reference commands for altitude and velocity (Case 2) [6]. Parameters for ATP and the basic TLC frame are given in Table II. Parameters for ESO are all set as $\beta_{i1}=\beta_{i2}=15$, $\alpha_i=0.5$, $\delta_i=0.01$, $i=V,h,\gamma,\alpha,Q$, which shows great parameter adaption property.

In Case 1, the altitude command is given to let the vehicle climb from 85000 ft to 95000 ft, whereas the velocity command is generated by solving the air density model to maintain constant dynamic pressure at 2000 psf. Under no uncertainty, robust tracking results are depicted in Fig. 6. Both velocity and altitude trajectories are tracked well. Note that the response of the altitude exhibits a typical undershoot behavior due to the nonminimun phase feature as predicted in the open-loop analysis. To make the test more demanding, uncertainties are added next. Propulsive perturbations and variations in control effectiveness are included with 40% uncertainty, while external uncertainty is considered as (25). In this case both the basic TLC frame and the robust TLC scheme with ESO compensation provide stable tracking results, as shown in Figs. 7a and 7b, although the basic TLC frame exhibits a large tracking error in the velocity response. Increasing the external uncertainty in the pitch rate dynamics to $0.05\sin t$ yields comparison results in Figs. 7c and 7d. The basic TLC frame completely loses its control ability while the robust scheme still performs well due to ESO. The actual uncertainties in velocity and pitch rate dynamics and the corresponding estimated values are shown in Fig. 8, where the excellent estimation ability of ESO is exhibited.

Case 2 considers a more aggressive maneuver where the velocity and altitude commands are independently given as 1000 ft/s and 12000 ft, respectively. Uncertainties are set as the same with those in the first case. The robust tracking results are depicted in Fig. 9. Although the dynamic pressure exhibits a slightly large decrease, which may significantly affect the vehicle characteristics as shown in Fig. 3, the velocity and altitude tracking still remain excellent. The internal states such as the angle of attack chatter due to the uncertainties, but they all stay in admissible ranges.

TABLE II CONTROL PARAMETERS

Parameter	Value	Parameter	Value	Parameter	Value
r_V	0.15	ω_V	0.02	ξ_V	0.7
r_h	1	ω_h	0.02	ξ_h	0.7
r_γ	0.001	ω_γ	0.05	ξ_γ	1
r_α	0.05	ω_α	0.25	ξ_α	0.7
r_Q	0.5	ω_Q	1	ξ_Q	0.7

V. Conclusions

Robust control design is a fundamental issue for FAHV with multiple uncertainties. In this work, comprehensive flexibility effects and open-loop behavior analysis for the vehicle model are conducted, offering a better understanding of the complex vehicle features. For controller design, a robust control scheme that integrates a basic TLC frame and the ESO technique is proposed. Furthermore, a uniform nonlinear uncertainty model is developed, which can represent all external disturbances and typical internal uncertainties such as propulsive perturbations and variations in control effectiveness. Comparison simulation demonstrates the great tracking performance and uncertainty rejection ability of the proposed robust control scheme.

Acknowledgment

This work is supported by the grants of National Natural Science Foundation of China (No. 61273149, 61203003) and the Special Project for Innovation Methods of MOST No. 2012IM010200 and No. B1320133020.

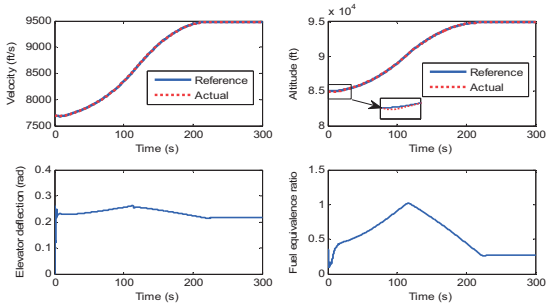

Fig. 6 Robust tracking results in Case 1 with no uncertainty.

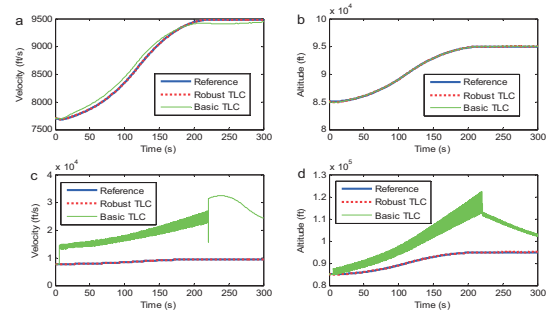

Fig. 7 Comparison simulations with different uncertainty levels in Case 1.

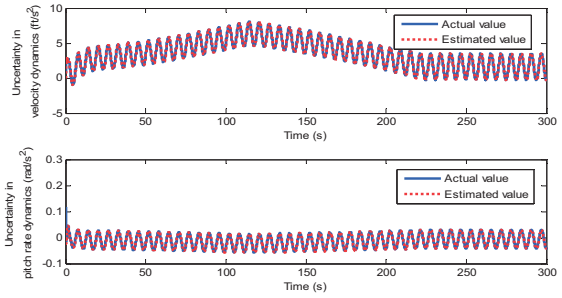

Fig. 8 Actual uncertainties and their estimated values by ESO in Case 1.

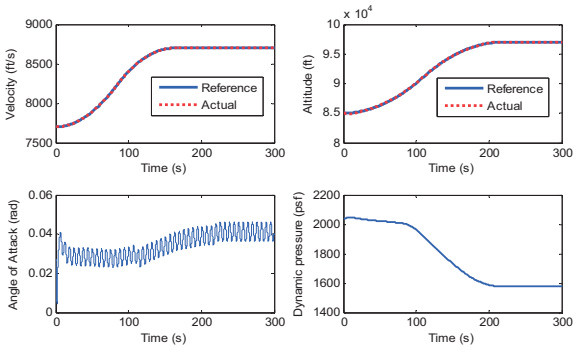

Fig. 9 Robust tracking results in Case 2 with uncertainties.

References

[1] M. A. Bolender and D. B. Doman, "Nonlinear longitudinal dynamical model of an air-breathing hypersonic vehicle," *Journal of Spacecraft and Rockets*, vol. 44, no. 2, pp. 374-387, March-April 2007.

[2] M. Mirmirani, C. Wu, A. Clark, S. Choi, and R. Colgren, "Modeling for control of a generic airbreathing hypersonic vehicle," *AIAA Guidance, Navigation and Control Conference and Exhibit*, AIAA 2005-6256, 15-18 August 2005.

[3] Z. D. Wilcox, W. MacKunis, S. Bhat, R. Lind, and W. E. Dixon, "Lyapunov-based exponential tracking control of a hypersonic aircraft with aerothermoelastic effects," *Journal of Guidance, Control, and Dynamics*, vol. 33, no. 4, pp. 1213-1224, July-August 2010.

[4] X. X. Hu, L. G. Wu, C. H. Hu, and H. J. Gao, "Adaptive sliding mode tracking control for a flexible air-breathing hypersonic vehicle," *Journal of the Franklin Institute*, vol. 349, no. 2, pp. 559-577, March 2012.

[5] J. T. Parker, A. Serrani, S. Yurkovich, M. A. Bolender, and D. B. Doman, "Control-oriented modeling of an air-breathing hypersonic vehicle," *Journal of Guidance, Control, and Dynamics*, vol. 30, no. 3, pp. 856-869, May-June 2007.

[6] L. Fiorentini, A. Serrani, M. A. Bolender, and D. B. Doman, "Nonlinear robust adaptive control of flexible air-breathing hypersonic vehicles," *Journal of Guidance, Control, and Dynamics*, vol. 32, no. 2, pp. 401-416, March-April 2009.

[7] M. Kuipers, M. Mirmirani, P. Ioannou, and Y. Huo, "Adaptive control of an aeroelastic airbreathing hypersonic cruise vehicle," *AIAA Guidance, Navigation and Control Conference and Exhibit*, AIAA 2007-6326, 20-23 August 2007.

[8] J. Levin, P. Ioannou, and M. Mirmirani, "Adaptive mode suppression scheme for an aeroelastic airbreathing hypersonic cruise vehicle," *AIAA Guidance, Navigation and Control Conference and Exhibit*, AIAA 2008-7137, 18-21 August 2008.

[9] J. J. Zhu, B. D. Banker, and C. E. Hall, "X-33 ascent flight control design by trajectory linearization-a singular perturbation approach," *AIAA Guidance, Navigation and Control Conference and Exhibit*, AIAA 2000-4159, 14-17 August 2000.

[10] Y. Liu and J. J. Zhu, "Regular perturbation analysis for trajectory linearization control," *American Control Conference*, July 11-13 2007.

[11] R. Huang, Y. Liu, and J. J. Zhu, "Guidance, navigation, and control system design for tripropeller vertical-takeoff-and-landing unmanned air vehicle," *Journal of Aircraft*, vol. 46, no. 6, pp. 1837-1856, November-December 2009.

[12] J. J. Zhu, "PD-spectral theory for multivariable linear time-varying systems," *Proceedings of the 36th IEEE CDC*, December 1997.

[13] H. Buschek and A. J. Calise, "Uncertainty modeling and fixed-order controller design for a hypersonic vehicle model," *Journal of Guidance, Control, and Dynamics*, vol.20, no. 1, pp. 42-48, January-February 1997.

[14] J. Q. Han, *Active Disturbance Rejection Control Technique-the Technique of Estimating and Compensating the Uncertainties*, National Defense Industry Press, Beijing, China, 2009, (In Chinese).

[15] Z. Q. Gao, Y. Huang, and J. Q. Han, "An alternative paradigm for control system design," *Proceedings of the 40th IEEE CDC*, 2001.